PyQM/MM: a Python Interface for ONIOM(QM:MM) Calculations with the AMOEBA09 Polarizable Force Field to Study the Chemical Processes in the Interstellar Medium

P. V. G. M. Rathnayake,[a] W. M. C. Sameera,[b,c] Naoki Watanabe,[b]*

[a]School of Chemistry, The University of Sydney, Sydney, New South Wales 2006, Australia.

[b]Institute of Low Temperature Science, Hokkaido University, N19-W8, Kita-ku, Sapporo, Hokkaido 060-0819, Japan. *E-mail: wmcsameera@lowtem.hokudai.ac.jp*

[c]Department of Chemistry, University of Colombo, Colombo 00300, Sri Lanka. *E-mail: wmcsameera@chem.cmb.ac.lk*

Abstract

We have developed a Python interface, PyQM/MM, to perform ONIOM(QM:MM) calculations with the AMOEBA09 polarizable force field. The ONIOM(QM:MM) implementation in PyQM/MM uses the Gaussian16 program for quantum mechanical (QM) computations and the Tinker program for molecular mechanics (MM) computations with the AMOEBA09 polarizable

force field. We have used PyQM/MM, employing ONIOM(QM:AMOEBA09) method, to calculate binding energy of SH and OH radicals on amorphous solid water (ASW). Computed binding energies of SH radical are in the range of 0.10-0.36 eV, where the average binding energy is 0.22 eV. Compared to SH radical, OH radical binding energies are stronger (0.21 – 0.52 eV, and the average value is 0.36 eV). We propose that both SH and OH radicals adsorb on ASW, and SH radical binding preference is smaller than OH radical. Also, we have rationalized the mechanism for the reaction between OH anion and CO in ice using ONIOM(wB97X-D:AMOEBA09) method. The computed reaction mechanism showed a relatively low energy path to form HC(O)OH, where the OH anion is recovered during the reaction. In contrast, the reaction between OH radical CO gives rise to HOCO radical. We propose that OH anions and OH radicals in interstellar ices can react with the molecules trapped in ices to synthesize complex organic molecules. These examples evidence that PyQM/MM is a user-friendly strategy to perform ONIOM(wB97XD:AMOEBA09) calculations to study chemical processes in the interstellar medium.

Introduction

Quantum mechanics (QM) has been the most successful approach in calculating the potential energy surfaces (PES) of molecular systems and their properties. Modern computational methods, employing QM methods, can calculate the stationary points on the PESs, specifically local minima (LM) or transition states (TS).[1-3] The computational cost is very high for complex molecular systems with many atoms if a QM method is used. Thus, quantum mechanics/molecular mechanics (QM/MM) methods have been developed.[4-9] In a QM/MM calculation, the electronically important part of the molecular system, binding site or active site, for instance, is calculated using a QM

method. The remining part of the molecular system is calculated using a MM method. Therefore, the QM/MM methods give accurate molecular structures and properties at a low computational cost. In a QM/MM calculation, the Hamiltonian operator of the molecular system can be defined as;

$$\hat{H} = \hat{H}_{QM} + \hat{H}_{MM} + \hat{H}_{Int} \quad \text{--(1)}$$

Where the $\hat{H}_{QM}$ is the Hamiltonian operator of the QM region, $\hat{H}_{MM}$ is the Hamiltonian operator of the MM region, and the $\hat{H}_{Int}$ represents the interactions between the QM and MM regions. Then, total energy can be written as;

$$E_{Total}(QM{:}MM) = E_{QM}(QM) + E_{MM}(MM) + E_{Int}(QM{:}MM) \quad \text{--(2)}$$

In this equation, the labels in parenthesis describe the region of the molecular system, while the labels in subscript denote the computational method. In the our own n-layer integrated molecular orbital molecular mechanics (ONIOM) method,[10-15] the $E_{Int}(QM{:}MM)$ term of the equation (2) is calculated by subtracting the internal energy of the real and the model systems;

$$E_{Int}(QM{:}MM) = E_{MM}(QM{:}MM) - [E_{MM}(QM) + E_{MM}(MM)] \quad \text{--(3)}$$

Then, the total energy of the ONIOM(QM:MM) method becomes;

$$E_{Total}(QM{:}MM) = E_{QM}(QM) + E_{MM}(QM{:}MM) - E_{MM}(QM) \quad \text{--(4)}$$

Similarly, the ONIOM(QM:MM) gradients and hessian can be calculated;

$$G_{ONIOM}(QM{:}MM) = G_{QM}(QM) \times J + G_{MM}(QM{:}MM) - G_{MM}(QM) \times J \quad \text{--(5)}$$

$$H_{ONIOM}(QM{:}MM) = J^T \times H_{QM}(QM) \times J + H_{MM}(QM{:}MM) - J^T \times H_{MM}(QM) \times J \quad \text{--(6)}$$

Where $J = \frac{\partial(real\ coord.)}{\partial(model\ coord.)}$ --(7)

The ONIOM(QM:MM) method have been used in modelling complex molecular systems in chemistry, biology, and materials science.[13] One of the present challenges is to use modern polarizable force fields with ONIOM(QM:MM) calculations. In this direction, we have been developing computational tools.[16-18] In the present work, we have introduced a python interface for substantive QM/MM calculations, the so-called PyQM/MM. In this implementation, QM calculations are performed by the Gaussian16 program,[19] while MM calculations are performed by the Tinker program (version 8.10),[20,21] employing the AMOEBA09[22-24] polarizable force field. Other polarizable or fixed charged models in the Tinker program can also be used for the MM calculations. PyQM/MM does not require third-party packages and works with the Python version 3.6 or higher. The PyQM/MM interface is available free of charge for academic users and can be downloaded at https://github.com/WMCSameeraGroup/pyqmmm. A brief description of PyQM/MM is given below.

PyQM/MM

In order to use PyQMMM, three input files are needed. (1) Gaussian16 input file with the "external" keyword, specifying the PyQM/MM executable file path. (2) params.dat file specifying

the location of the MM parameters file. (3) atomtypes.dat file containing MM atom types. A detailed description can be found in the supplementary data. Once Gaussian16 executes ONIOM(QM:MM) calculation employing the PyQM/MM as the "external" program, a text file with the extension of EIn is created. This file consists of the Cartesian coordinates of the molecular structure, atom types, and the connectivity of the atoms. PyQM/MM converts the information in the EIn file into the Tinker compatible input file with the extension of XYZ. Then, PyQM/MM executes the Tinker MM calculations and reads the MM output data. Finally, PyQM/MM constructs the Gaussian16 compatible data source file with the EOu extension. After that, Gaussian16 collects data from the EOu file and proceeds.

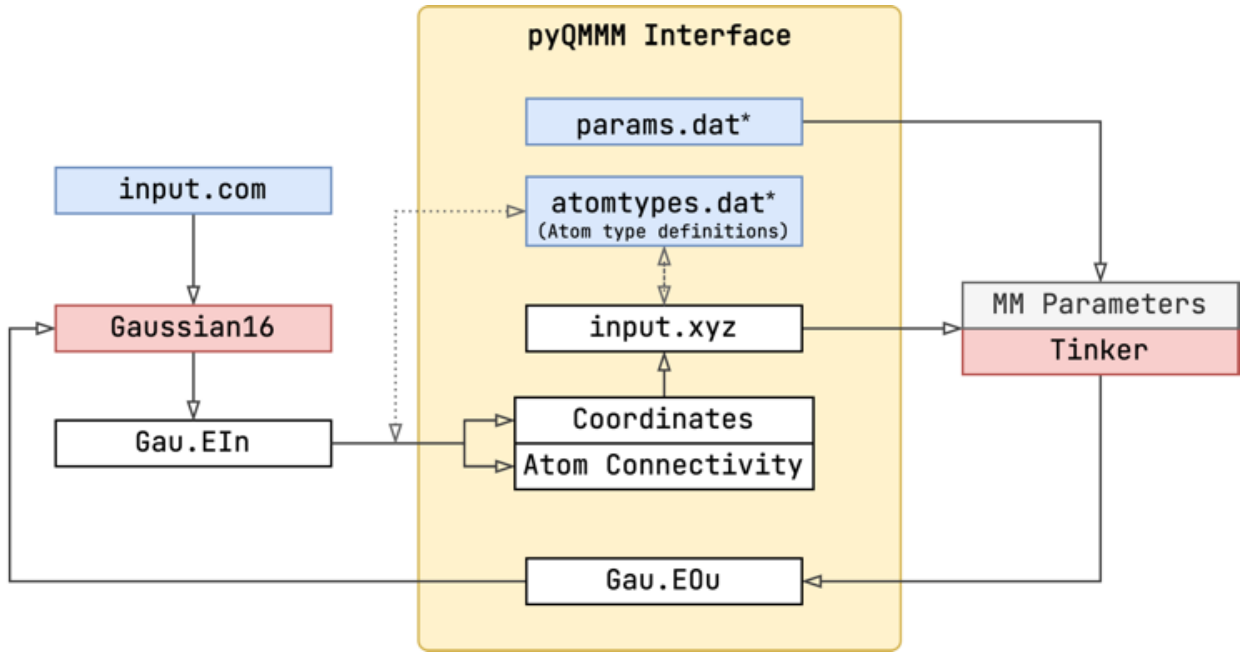

Figure 1. PyQM/MM interface between the Gausian16 and Tinker programmes.

The following section described the applications of PyQM/MM, where our interest is to employ ONIOM(QM:AMOEBA09) method to study radical processes in the interstellar medium (ISM).

Applications of PyQM/MM

Radical species in the ISM play a vital role in forming complex organic molecules (COMs).[25-27] To understand the chemical evolution in the ISM, it is essential to understand the elementary radical process, such as radical adsorption, diffusion and chemical reactions on the ice mantles of interstellar grains.[28-31] Hydrogenation (e.g. $O + H \rightarrow OH$, $CO + H \rightarrow HCO$) and photodissociation of small molecules (e.g., H_2O, CH_4, H_2CO, CH_3OH, NH_3) in ice mantles in the ISM give rise to the primary radicals, specifically H, OH, CO, HCO, CH_3O, CH_2OH, CH_3, NH, and NH_2. Accumulation of the primary radicals on the icy grain surfaces may occur at very low temperatures (e.g., 10 K) in dark clouds. At 10K, only H atoms may diffuse on grain surfaces and react with the radicals and molecules adsorbed on ices to make relatively large molecules or radicals. Other primary radicals diffused on ices at relatively high temperatures, the so-called warming-up stage to form the COMs when they encounter molecules or radicals.

Our recent studies focused on the behaviour of OH radicals on ices.[32,33] Experiments created OH radicals on ices by photodissociation of H_2O under the interstellar conditions. Computed ground and excited states potential energy surfaces of OH-$(H_2O)_n$ complexes suggested that one-photon absorption of the OH radical can stimulate the desorption from ices. Also, computational studies indicated that the binding energy of the OH radical on ice is sensitive to the dangling atoms, in particular, hydrogen (*d*-H) or dangling oxygen (*d*-O) at the binding site. Thus, a range of binding energies was obtained. The computed binding energies of the other radical species are also in a broad range, CH_3O[34]: 0.10–0.50 eV, PH_2[35]: 0.13–0.21 eV, PH[35]: 0.10–0.19 eV, P[35]: 0.07–0.16 eV, and OCSH[36]: 0.19–0.46 eV. Binding energy OH radical is relatively strong, and therefore OH radicals adsorb on the interstellar ices at low temperatures. If such an OH radical encounters an

electron, an OH anion can be formed. According to our *ab-initio* MD simulations, OH anions on ice react with the surface water molecules and drive the OH anion towards ice bulk through the proton hole transfer mechanism.[37,38] The PHT process gives rise to a negative current, which we have detected at low temperatures.

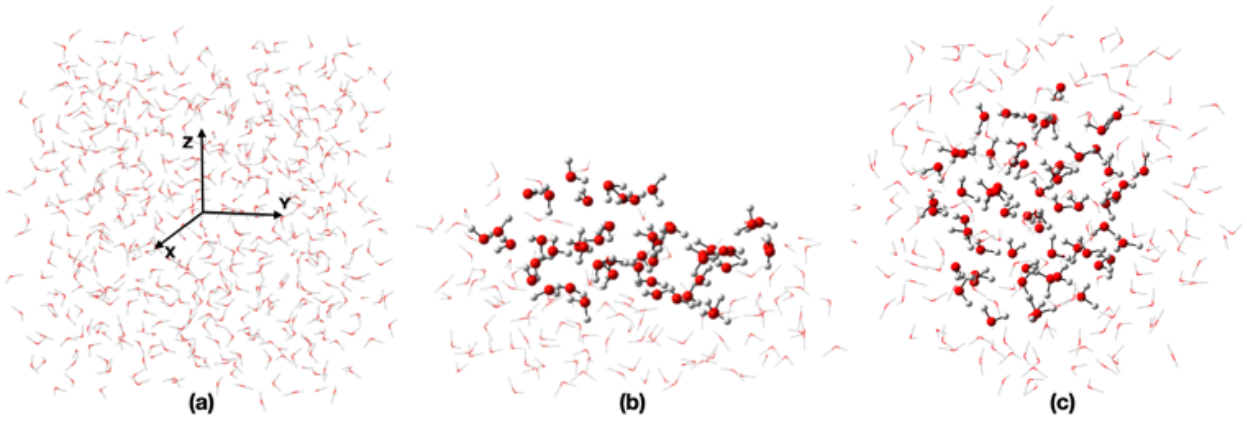

Figure 2. (a) The unit cell of the two or three-dimensional periodic structure (25 x 25 x 25 Å). (b) Ice surface and (c) ice bulk cluster models for ONIOM(QM:MM) calculations. The ONIOM-high layer is shown in "ball and stick", and the ONIOM-low layer is shown in "wireframe".

In the present paper, we have compared the binding energy of SH and OH radicals on amorphous solid water, ASW. Also, we have calculated the potential energy surfaces for the reactions in ices; OH^- + CO and $OH^\cdot$ + CO. We have chosen CO because it is one of the abundant molecules in the ISM.

Computational Methods

Preparation of ice model structures

Molecular dynamics (MD) simulations were performed using the Tinker package (version 8.10) using the AMOEBA09 force field. The temperature and pressure were maintained using the Andersen thermostat and Berendsen barostat, respectively. All MD simulations were performed under 1 atm pressure and the time step of 1 fs.

Ice surface model structure

A two-dimensional periodic structure (25 x 25 x 25 Å), consisting of 493 H2O molecules (density 0.94 g/mol), was prepared (Figure 2a) energy minimization was performed using the AMOEBA09 force field**.** Then, a 5 ps long NVT run followed by 5 ps long NPT run were carried out, where the temperature was maintained at 300 K. After that, the temperature was set to 10 K, and the NVT run followed by NPT was carried out, where each simulation was 5 ps long. Then, the resulting structure was optimized using the AMOEBA09 force field. Starting from the optimized structure, a cluster model consisting of 240 H_2O molecules was prepared (Figure 2b). Moreover, 50 H_2O molecules in this cluster model were defined as the ONIOM high-layer, while the remaining 190 H_2O molecules were defined as the ONIOM low-layer.

Ice bulk model structure

A three-dimensional periodic structure (25 x 25 x 25 Å), consisting 493 H_2O molecules (density 0.94 g/mol) was prepared and the structure was optimized. Then, MD simulations were performed as described above, and a cluster model consisting 240 H_2O molecules was prepared (Figure 2c),

where 50 H_2O molecules are included in the ONIOM-high layer, and the remaining 190 H_2O molecules are in the ONIOM low-layer.

ONIOM(QM:MM) structure optimizations

Geometry optimizations were performed using the PyQM/MM interface. Density functional theory (DFT), employing the wB97X-D functional,[39] and the 6-31G*or 6-31+G* basis sets[40-42] were used for the ONIOM high-layer. The AMOEB09 polarizable force field was used for the ONIOM low-layer. The AMOEBA09 atom types employed in this study are summarized in Table S1. Atoms in the ONIOM low-layer were frozen during the structure optimizations to avoid ice structure deformations. Vibrational frequency calculations were performed to confirm that the optimized structures were local minima (i.e., no imaginary frequencies) and to calculate zero-point energies. The potential energy of the optimized structures was calculated as ONIOM(wB97X-D/def2-TZVP[43]:AMOEBA09) single-point energy calculations. Binding energies of SH or OH radical on ices were calculated using the following formula;

$$\text{Binding energy} = \left| E_{(ice-radical)} - E_{ice} - E_{radical} \right| \quad \text{--(7)}$$

In this equation, $\boldsymbol{E_{(ice-radical)}}$ is the total energy of an optimized radical-ice complex. $\boldsymbol{E_{ice}}$ term is denoted the total energy of the ice cluster model, and $\boldsymbol{E_{radical}}$ is the total energy of the ice cluster model, and $\boldsymbol{E_{radical}}$ is the total energy of the optimized SH or OH radicals.

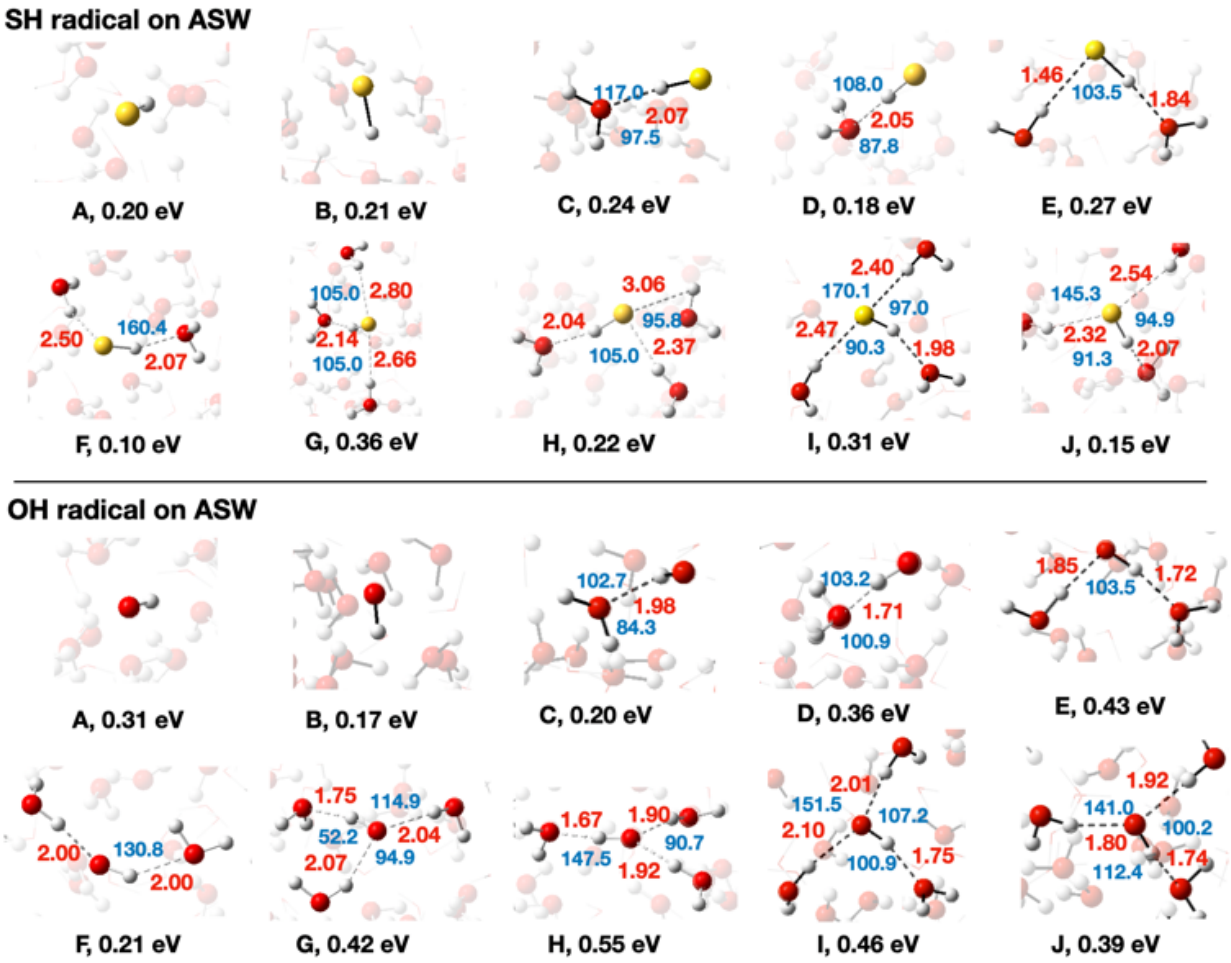

Figure 3. Optimized structures of the SH and OH radicals on ASW. For simplicity, only the binding pocket of the QM region is shown. Binding energies are in eV, bond lengths are in Å, and bond angles are in degrees.

Results and discussion

Water molecules on the top layer of ice surface can make three hydrogen bonds at most with the water molecules in ice, and leave a *d*-Os or *d*-Hs on the surface. The radical or molecular species interact with the *d*-Os and *d*-Hs. Thus, we have chosen ten binding sites, showing various

combinations of *d*-Os and *d*-Hs in the binding sites. Optimized structures of the SH and OH radicals bound ASW and computed binding energies are shown in Figure 3 and Figure 4.

In A and B, the SH radical does not interact with the *d*-Os or *d*-Hs on ice, and the computed binding energies are 0.20 and 0.21 eV, respectively. Relatively similar binding energies can be seen for C (0.24 eV) and D (0.18 eV), where the SH radical is attached to a *d*-O on ice. In the case of E (0.27 eV) and F (0.10 eV), the S-H radical interact with two dangling atoms on ice (i.e., one *d*-H and one *d*-O). The SH radical in G-J binding sites interact with three dangling atoms on ice (i.e., one *d*-H and two *d*-O), and the calculated binding energies are 0.36 (G), 0.22 (H), 0.31 (I), 0.15 eV (J). Overall, calculated binding energies of SH radical on ASW are in the range of 0.10-0.36 eV, and the average binding energy is 0.22 eV. The binding site G shows the strongest binding energy (0.36 eV), while the binding site F shows the weakest binding energy (0.10 eV).

Then, we have calculated the binding energies of OH radical on the binding sites A-J. Computed OH radical bonding energies are summarized in Figures 3 and 4. Compared to the SH radical binding energies, the OH radical binding energies are relatively strong (except B and C). The binding energies of the OH radical are in the range of 0.17 – 0.55 eV, which is wider than the SH radical (0.10-0.36 eV). The average binding energy is 0.35 eV, which is in agreement with the previous studies,[18,32] and is relatively larger than that of the SH radical (0.22). Thus, we concluded that the SH radical bonding energy on ASW is relatively weak compared to that of the OH radical.

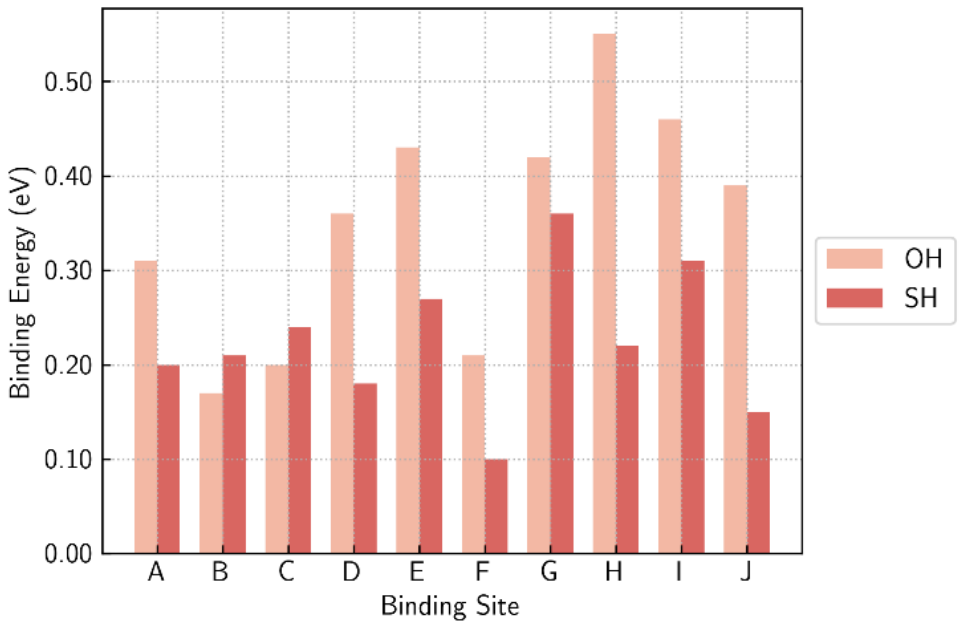

Figure 4. Calculated binding energies of an SH and an OH radical on ASW from ONIOM(wB97X-D/Def2-TZVP:AMOEBA09) method.

The ONIOM-high later of the ice cluster models consists of 50 H_2O molecules. To check whether the size of the ONIOM-high later has an effect on the computed binding energy, we have compared the binding energies from ONIOM(wB97XD/def2-TZVP:AMOEBA09) and wB97XD/def2-TZVP methods (Figure S1). In general, the two approaches gave consistent binding energies, where the maximum discrepancy is 0.09 eV for the SH radical, and 0.11 for the OH. Thus, the electronic effects of the atoms in the MM region are not large, and the size of the ONIOM-high later is suitable for calculating binding energies of SH or OH radical on ASW.

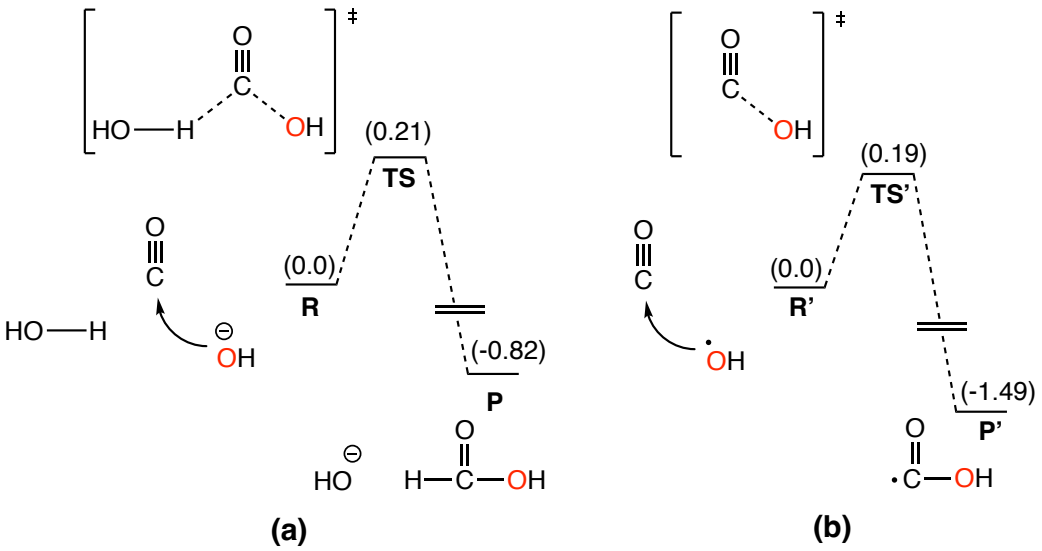

Figure 5. PES for the reaction between (a) OH anion and CO and (b) OH radical and CO in ice from ONIOM(wB97XD/def2-TZVP:AMOEBA09) method. Potential energies (including ZPE) are in eV. Molecular structures of the optimized stationary points are shown in Figure 6.

OH^- + CO reaction in ices

Next, we turned our attention to the chemical reactions in ice. If OH anions are formed on installer ices, they can be transmitted in ice bulk.[37-38] When an OH anion in ices meets an organic molecule trapped in ice, COMs may be formed. To test this hypothesis, the reaction mechanism between an OH anion and a CO in ice was calculated using ONIOM(wB97XD/def2-TZVP:AMOEBA09) method. The computed PES is shown in Figure 5a, and the molecular structures of the stationary points are shown in Figure 6.

The starting point of the potential energy surface is the local minimum **R** (Figure 6), where the distance between OH anion and CO, i.e., C-O1, is 2.46 Å. At the transition state geometry (**TS1**),

C-O1 distance became shorter (1.88 Å). The computed reaction barrier is 0.21 eV. The product of the reaction, HC(O)OH (**P**), is 0.82 eV more stable than **R**, where the C-O1 distance is 1.33 Å. During the C-O1 formation, the C atom abstracts a proton from a neighbouring water molecule, and the OH anion is recovered. Thus, the OH anion acts as the catalyst to convert CO into formic acid in ice, which is a known molecule in the ISM.

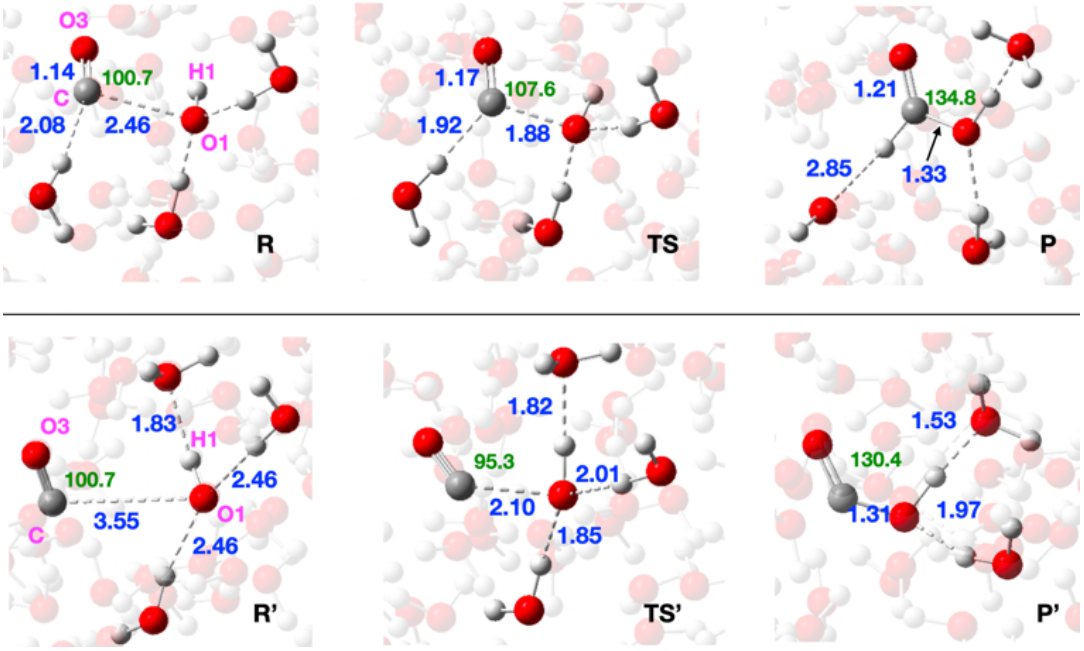

Figure 6. Molecular structures of the stationary points **R**, **TS**, **P**, **R'**, **TS'**, and **P'**. Bond distances are in Å, and bond angles are in degrees.

OH^- + CO_2 reaction in ices

Then, we have computed the potential energy surface for the reaction between OH radical and CO in ice (Figure 5b). OH radicals in interstellar ices can be formed through the photodissociation of water. In the local minimum of the reactant complex, **R'**, the distance between CO and OH (i.e.,

C-O1) is 3.55 Å. The computed barrier for the reactions is 0.19 eV, where the C-O1 distance at the transition state geometry, **TS'**, is relatively shorter (2.10 Å). The product of the reaction, HOCO radical (**P'**) is -1.49 eV more stable than the reactant complex.

Based on ONIOM(wB97XD/def2-TZVP:AMOEBA09) calculations, we concluded that the reaction between OH anion and CO in ice produces HC(O)OH, while the reaction between OH radical and CO produces HOCO radical. Both reactions may operate in interstellar ices that may contribute for the formation of the COMs.

Conclusions

PyQM/MM combines the AMOEBA09 polarizable forcefield with the two-layer ONIOM method. We have used the ONIOM(QM:AMOEBA09) implementation in PyQM/MM to study SH and OH radical binding energies on ASW. A range of binding energies was found; SH: 0.10-0.36 eV and OH: 0.21 – 0.52 eV. The calculated average binding energies, 0.22 eV of SH and 0.36 eV of OH indicated binding preference for OH. Also, ONIOM(QM:AMOEBA09) calculations suggested that the reaction between an OH anion and a CO molecule in ice gives formic acid through a low energy barrier, where OH anion acts as the catalyst. In contrast, the reaction between OH radical and CO produces HOCO radical through a low energy barrier. Therefore, we suspect that OH anions or OH radicals in ice play a role in COMs formation in the ISM. These examples evidence that the ONIOM(QM:AMOEBA09) method is suitable for modelling chemical processes in the ISM. In the future, ONIOM(QM:AMOEBA09) method can applied for modelling large molecular systems in organic, biochemical, and materials science.

Author Contributions

MR have written the codes. MR and WMC have performed calculations. WMC designed the project and wrote the original manuscript. MR and NW revised the manuscript. All authors have given approval to the final version of the manuscript.

Conflicts of interest

There are no conflicts to declare.

Acknowledgements

This work was partly supported by JSPS KAKENHI Grant Numbers JP19K03940 and JP21H05416 (to W.C.M.S.), JP17H06087 (to N.W.). Supercomputing resources at the Institute for Information Management and Communication at Kyoto University in Japan and the Institute for Molecular Science (IMS) in Japan are acknowledged.

References

1 H. B. Schlegel, *WIREs Comput. Mol. Sci.*, 2011, **1**, 790-809.

2 W. M. C Sameera, S. Maeda, and K. Morokuma, *Acc. Chem. Res.*, 2016, **49**, 763-773.

3 W. M. C. Sameera, A. K. Sharma, S. Maeda and K. Morokuma, *Chem. Rec.*, 2016, **16**, 2349-2363.

4 S. Lifson and A. Warshel, *J. Chem. Phys.,* 1968, **49**, 5116–5129.

5 B. Honig and M. Karplus, *Nature,* 1971, **229**, 558–560.

6 A Warshel and M. Levitt, *J. Mol. Biol.,* 1976, **103**, 227–249.

7 F. Maseras and K. Morokuma, *J. Comput. Chem.,* 1995, **16**, 1170–1179.

8 J. L. Gao, *Acc. Chem. Res.,* 1996, **29**, 298–305.

9 H. M. Senn and W. Thiel, *Angew. Chem., Int. Ed.,* 2009, **48**, 1198–1229.

10 F. Maseras and K. Morokuma, *J. Comput. Chem.*, 1995, **16**, 1170–1179.

11 M. Svensson, S. Humbel, R. D. J. Froese, T. Matsubara, S. Sieber and K. Morokuma, *J. Phys. Chem.*, 1996, **100**, 19357–19363.

12 T. Vreven and K. Morokuma, *Annu. Rep. Comput. Chem.*, 2006, 2, 35–51.

13 L. W. Chung, W. M. C. Sameera, R. Ramozzi, A. J. Page, M. Hatanaka, G. P. Petrova, T. V. Harris, X. Li, Z. F. Ke, F. Y. Liu, H. -B. Li, L. N. Ding, and K. Morokuma, *Chem. Rev.*, 2015, **115**, 5678–5796.

14 J. R-G. Pedregal, I. Funes-Ardoiz, G.Sciortino, J. E. Sánchez-Aparicio, G. Ujaque, A. Lledós, J. D. Maréchal, F. Maseras, F, *J Comput. Chem.*, 2019, **40**, 381-386.

15 W. M. C. Sameera and F. Maseras, *WIREs Comput. Mol. Sci.*, 2012, **2**, 375–385.

16 W. M. C. Sameera, B. Senevirathne, S. Andersson, F. Maseras, and G. Nyman. *J. Phy. Chem. C*, 2017, **121**, 15223-15232.

17 W. M. C. Sameera and F. Maseras, *J. Chem. Info. Model.*, 2018, **58**, 1828-1835.

18 W. M. C. Sameera and F. Maseras, *Phys. Chem. Chem. Phys.*, 2011, **13**, 10520-10526.

19 M. J. Frisch, G. W. Trucks , H. B. Schlegel , G. E. Scuseria, M. A. Robb, J. R. Cheeseman, G. Scalmani, V. Barone, G. A. Petersson, H. Nakatsuji, X. Li, M. Caricato, A. V. Marenich, J. Bloino, B. G. Janesko, R. Gomperts, B. Mennucci, H. P. Hratchian, J. V. Ortiz, A. F. Izmaylov, J. L. Sonnenberg, D. Williams-Young, F. Ding, F. Lipparini, F. Egidi, J. Goings, B. Peng, A. Petrone, T. Henderson, D. Ranasinghe, V. G. Zakrzewski, J. Gao, N. Rega, G. Zheng, W. Liang, M. Hada, M. Ehara, K. Toyota, R. Fukuda, J. Hasegawa, M. Ishida, T. Nakajima, Y. Honda, O. Kitao, H. Nakai, T. Vreven, K. Throssell, J. A. Montgomery, Jr., J. E. Peralta, F. Ogliaro, M. J. Bearpark, J. J. Heyd, E. N. Brothers, K. N. Kudin, V. N.

Staroverov, T. A. Keith, R. Kobayashi, J. Normand, K. Raghavachari, A. P. Rendell, J. C. Burant, S. S. Iyengar, J. Tomasi, M. Cossi, J. M. Millam, M. Klene, C. Adamo, R. Cammi, J. W. Ochterski, R. L. Martin, K. Morokuma, O. Farkas, J. B. Foresman and D. J. Fox, *Gaussian 16, Revision C.01*, Gaussian, Inc, Wallingford CT, 2016.

20 J. W. Ponder and F. M. Richards, *J. Comput. Chem.*, 1987, **8**, 1016–1024.

21 C. E. Kundrot, J. W. Ponder and F. M. Richards, *J. Comput. Chem.*, 1991, **12**, 402–409.

22 J. W. Ponder and D. A. Case, *Adv. Protein Chem.*, 2003, **66**, 27–85.

23 P. Y. Ren and J. W. Ponder, *J. Phys. Chem. B*, 2003, **107**, 5933– 5947.

24 P. Y. Ren, and J. W. Ponder, *J. Comput. Chem.*, 2002, **23**, 1497–1506.

25 M. Guélin and J. Cernicharo, *Space Sci.*, 2022, **9**, 787567.

26 E. Herbst, and E. F. van Dishoeck, *Annu. Rev. Astron. Astrophys.*, 2009, **47**, 427–480.

27 W. M. C. Sameera, B. Senevirathne, T. Nguyen, Y. Oba, A. Ishibashi, M. Tsuge, H. Hidaka, and N. Watanabe, *Astron. Space Sci.* 2022 (Accepted) DOI: 10.3389/fspas.2022.890161

28 E. Herbst and R. T. Garrod, *Front. Astron. Space Sci.*, 2022, 8:789428.

29 R. T. Garrod and E. Herbst, *Astron. Astrophys.*, 2006, **457**, 927-936.

30 K. -J, Chuang, G. Fedoseev, S. Iopporo, E. F. van Dishoeck, and H. Linnartz, *Mon. Not. R. Astron. Soc.*, 2016, **455**, 1702–1712.

31 K. I. Öberg, R. T. Garrod, E. F. van Dishoeck and H. Linnartz, *Astron. Astrophys.*, 2009, **504**, 891-913.

32 A. Miyazaki, N. Watanabe, W. M. C. Sameera, Y. Nakai, M. Tsuge, T. Hama, H. Hidaka and A. Kouchi, *Phys. Rev. Lett. A*, 2020, **102**, 052822.

33 M. Tsuge and N. Watanabe, *Acc. Chem. Res.*, 2021, **54**, 471-480**.**

34 W. M. C. Sameera, B. Senevirathne, S. Andersson, M. Al-lbadi, H. Hidaka, A. Kouchi, G. Nyman and N. Watanabe, *J. Phy. Chem. A*, 2021, **125**, 1, 387–393.

35 T. Nguyen, Y. Oba, W. M. C. Sameera, A. Kouchi and N. Watanabe, *Astrophys. J.*, 2021. **198**, 73.

36 T. Nguyen, Y. Oba, W. M. C. Sameera, A. Kouchi and N. Watanabe, *Astrophys. J.*, 2021, **922**, 146.

37 N. Watanabe, W. M. C. Sameera, H. Hidaka, A. Miyazaki and A. Kouchi, *Chem. Phys. Lett.*, 2019, **737**, 136820.

38 K. Kitajima, Y. Nakai, W. M. C. Sameera, M. Tsuge, A. Miyazaki, H. Hidaka, A. Kouchi and N. Watanabe, *J. Phys. Chem. Lett.*, 2021, **12**, 1, 704–710.

39 J. -D. Chai and M. Head-Gordon, *Phys. Chem. Chem. Phys.*, 2008, **10**, 6615-6620.

40 R. Ditchfield, W. J. Hehre and J. A. Pople, *J. Chem. Phys.*, 1971, **54**, 724-728.

41 W. J. Hehre, R. Ditchfield and J. A. Pople, *J. Chem. Phys.*, 1972, **56**, 2257-2261.

42 P. C. Hariharan and J. A. Pople, *Theor. Chim. Acta*, 1973, **28**, 213-222.

43 F. Weigend and R. Ahlrichs, *Phys. Chem. Chem. Phys.*, 2005, **7**, 3297-3305.